Journal of the Korean Crystal Growth and Crystal Technology
Vol. 16, No. 1 (2006) 12-19

Metalorganic chemical vapor deposition of semiconducting ZnO thin films and nanostructures

Sang-Woo Kim†

School of Advanced Materials and System Engineering, Kumoh National Institute of Technology, Gumi 730-701, Korea

(Received November 4, 2005)
(Accepted November 14, 2005)

Abstract Metalorganic chemical vapor deposition (MOCVD) techniques have been applied to fabricate semiconducting ZnO thin films and nanostructures, which are promising for novel optoelectronic device applications using their unique multifunctional properties. The growth and characterization of ZnO thin films on Si and SiO_2 substrates by MOCVD as fundamental study to realize ZnO nanostructures was carried out. The precise control of initial nucleation processes was found to be a key issue for realizing high quality epitaxial layers on the substrates. In addition, fabrication and characterization of ZnO nanodots with low-dimensional characteristics have been investigated to establish nanostructure blocks for ZnO-based nanoscale device application. Systematic realization of self- and artificially-controlled ZnO nanodots on SiO_2/Si substrates was proposed and successfully demonstrated utilizing MOCVD in addition with a focused ion beam technique.

Key words ZnO, Thin film, Nanostructure, MOCVD, FIB, Exciton, Nanodot, Quantum effects, Stimulated emission, Nanorod, Selective growth

1. Introduction

Recently, ZnO has attracted attention as a promising material for short-wavelength optical device applications due to the great advantage of having a large exciton binding energy (60 meV) [1], which is quite larger than those of other semiconductor materials with wide band gaps such as GaN (25 meV) and ZnSe (22 meV). Emission of ZnO-based semiconductors can cover the blue and UV spectrum range by doping Cd or Mg to ZnO [2-4], indicating that band-gap engineering can be effectively realized. In addition, ZnO possesses multifunctional characteristics such as semiconducting [5], piezoelectric [6], metallic [7], transparent [8], and magnetic properties [9]. In these regards, recently, studies on ZnO have been extensively underway. Due to the remarkable excitonic properties of ZnO such as large exciton binding energy and biexciton binding energy (15 meV) [10], strong exciton effects such as room temperature (RT) stimulated emission by inelastic exciton-exciton scattering have been reported [11-13]. Furthermore, many significant exciton effects promising for achieving large oscillator strength, significant nonlinear optical properties, and multiexciton interaction are expected in low-dimensional ZnO nanostructures because of enhancing exciton/biexciton binding energy [14, 15], resulting in radiative recombination with fast decay of carriers and observation of strong excitonic recombination even at RT.

To date, ZnO nanostructures such as nanowires, nanobelts, and nanoparticles have been reported [16-18]. However, there have been few studies on the formation of zero-dimensional ZnO structures using a conventional semiconductor growth method in spite of many extensive studies on compound semiconductors such as InAs and CdSe [19, 20]. In addition, in order to build nanostructure blocks for ZnO-based nanoscale device application as shown in Fig. 1, precise size and position control of nanostructures is essential. In this regard, the formation of highly ordered one- and two-dimensional ZnO nanodot arrays on focused ion beam (FIB)-nanopatterned substrates is reported in this work.

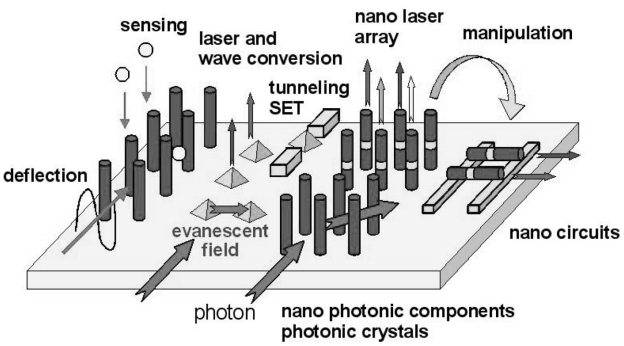

Fig. 1. Schematic image of ZnO-based nanostructure blocks for on-chip integrated nanoscale devices.

†Corresponding author
Tel: +82-54-478-7745
Fax: +82-54-478-7769
E-mail: kimsw@kumoh.ac.kr

2. Growth System

All depositions of ZnO thin films and nanostructures in this work have been carried out in a MOCVD system. Diethylzinc (DEZn) was used for a Zn source. For an oxygen source, nitrous oxide (N_2O) and nitrogen dioxide (NO_2) were introduced. The availability of large high-quality Si substrates as well as their low cost make it an attractive alternative substrate to sapphire for the growth of ZnO layers. However, the direct growth of high-quality ZnO on Si was found to be difficult, probably due to the larger value of the formation enthalpy of SiO_2 (–910.7 ± 1.0 kJ/mol) compared to that of ZnO (–350.46 ± 0.27 kJ/mol) [21] which makes it easier to form silicon dioxide. In addition, we could confirm that nucleation of ZnO is not efficient in the initial stage of growth due to deficient oxygen supply of the N_2O precursor. These problems can be overcome by direct growth of ZnO on Si substrates by using NO_2 [22], which was more reactive with DEZn compared to N_2O. This strong reactivity was preferable for the bonding of ZnO on Si, nevertheless prereaction in the gas phase during growth in the MOCVD reactor and the lower purity of NO_2 compared with N_2O for the oxygen source cannot be ignored. These facts mean that advantage and disadvantage in use of N_2O and NO_2 for an oxygen source is *vice-versa*.

3. MOCVD Growth of ZnO Thin Films on Si and SiO_2 Substrates

DEZn and NO_2 were used for growth of the ZnO on Si (111). Typical flow rates of DEZn and NO_2 for growth of ZnO on Si (111) were 2~4 and 100 μmol/min, respectively. Total pressure of the reactor was kept at 8 Torr and substrate temperatures were varied from 300~700°C. For the growths, electronic grade (6 N) N_2 gas was used instead of H_2 as the carrier gas to avoid etching of the surface of the ZnO layer.

Figure 2 shows the variation of the ZnO growth rate as functions of the flow rate of DEZn and growth temperature. By increasing the flow rate of DEZn, growth rate was linearly increased. On the other hand, the growth rate rapidly decreased with higher growth temperatures. The result is reasonable and common in MOCVD growth considering the enhancement of desorption probability of atomic radicals introduced into the MOCVD chamber at high substrate temperature. In addition, when the DEZn flow was increased, the *c*-axis oriented crystallinity was improved confirming by x-ray diffraction characterization. Photoluminescence (PL) spectra shown in Fig. 3 were measured at 9K. All the samples show a strong excitonic emission with no deep emission. Figure 3(a) compares the spectra for the ZnO samples grown at different flow rates of DEZn at 500°C. With the DEZn flow rate of 2 and 3 μmol/min the spectra are dominated by a D°X emission band. On the other hand, in the ZnO thin film grown with the DEZn flow rate of 4 μmol/min, bound exciton transition (IX) and its LO phonon replicas (IX-LOs) are dominant. Because these emissions are a special feature of ZnO on Si, they might be attributed to Si impurity bound exciton transition and its LO-phonon replicas or rotation domain structure-induced localized state bound exciton transition and its LO-phonon replicas [23]. In order to investigate the effect of growth temperature to optical qualities, the author also carried out PL measurements of the samples with different growth temperature from 300 to 700°C [Fig. 3(b)]. It is very difficult to observe a free exciton (EX) emission from the samples grown at 300 and 400°C. EX emission becomes stronger and the full-

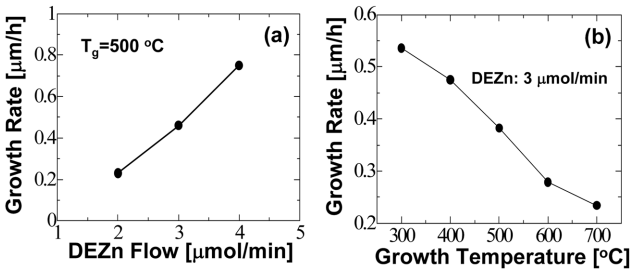

Fig. 2. Variation of the ZnO growth rate as a function of the flow rate of DEZn and growth temperature.

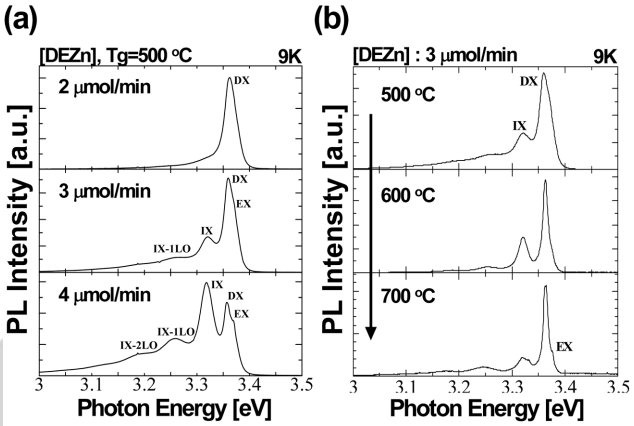

Fig. 3. (a) PL spectra measured at 9 K from the ZnO thin films with the DEZn flow rate of 2, 3, and 4 μmol/min and growth temperature of 500°C. (b) PL properties (9 K) of the ZnO thin films grown at 500, 600, and 700°C with a typical flow rate of 3 μmol/min.

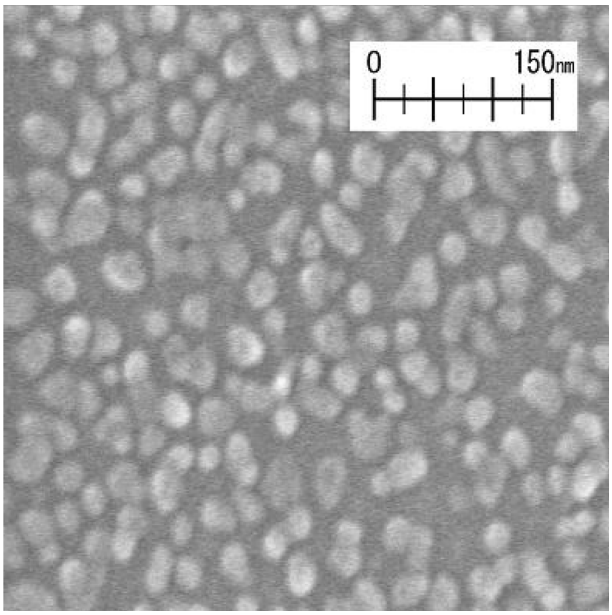

Fig. 4. Plan-view FE-SEM image of the nucleated ZnO nanocrystallites on SiO_2.

width half maximum value of the neutral donor-bound exciton (D^oX) emission band was reduced in the sample with higher growth temperature. Considering these facts, it could be suggested that high temperature growth can make incorporation of impurities (shallow donors) into ZnO becomes small.

Nucleation of ZnO crystallites on SiO_2 is not efficient at the initial stage. In addition, the nucleated ZnO crystallites have no specific epitaxial alignment with random distribution due to amorphous nature of SiO_2. Figure 4 shows a plan-view field-emission scanning electron microscopy (FE-SEM) image of the nucleated ZnO crystallites on Si with no wet and thermal treatments. ZnO nanosized crystallites with diameters of about 10~60 nm are clearly shown in the SEM image. This result is clear evidence that the behavior of ZnO growth follows the three-dimensional growth mode on SiO_2. This three-dimensional growth mode of ZnO on SiO_2 can be a promising technique to realize ZnO nanostructures with low-dimensional quantum characteristics.

4. Low-Dimensional Quantum Characteristics from Self-Organized ZnO Nanodots on SiO_2 Substrates

ZnO-nanodot structures were successfully realized in this work using three-dimensional growth behavior of ZnO on SiO_2 substrates. NO_2 gas for the oxygen source is more reactive than N_2O, which can supply for sufficient amount of oxygen atoms, was introduced in order to achieve effective quantum size effects from ZnO dots by the enhancement of crystallinity. The self-organized ZnO nanodots in this work were grown on thermally formed SiO_2 layers with a thickness of 25 nm on Si (111) substrates by MOCVD, where DEZn as a zinc source and reactive NO_2 gas as an oxygen source were used. The flow rates of DEZn and NO_2 were optimized as 3 and 100 μmol/min, respectively. The total pressure was fixed at 10 Torr at different temperatures at intervals of 50°C in the range of 450~600°C.

ZnO nanodots for the same growth time (30 s) at different growth temperatures with intervals of 50°C (from 400 to 500°C) were grown on SiO_2/Si substrates. The dot density decreases and the dot size increases with the increment of growth temperature from 450 to 600°C. Densities of the dots grown at 450, 500, 550, and 600°C were over 1×10^{11}, 1.2×10^{10}, 6.1×10^{9}, and 5.6×10^{9} cm^{-2}, respectively. In addition, maximum dot heights investigated by atomic force microscopy (AFM) were 5 (450°C), 5 (500°C), 10 (550°C), and 20 (600°C) nm. The increment of growth temperature usually increases the adatom diffusion length, leading to the increase of the dot size. As a result, the dot density decreases and the average size increases with increasing growth temperature. ZnO nanodots were also grown at 450 and 550°C for 90 s with the typical flow rates of DEZn and NO_2 being 3 and 100 mmol/min, respectively (Fig. 5). In the sample grown at 550°C, the dot density is 1.8×10^{11} cm^{-2}, the average height is 6 nm, and the average width is 31 nm. However, dot formation at relatively low growth temperature of 450°C is extremely dense and makes accurate measurements impossible.

PL spectra measured at 10 K from the ZnO thin film

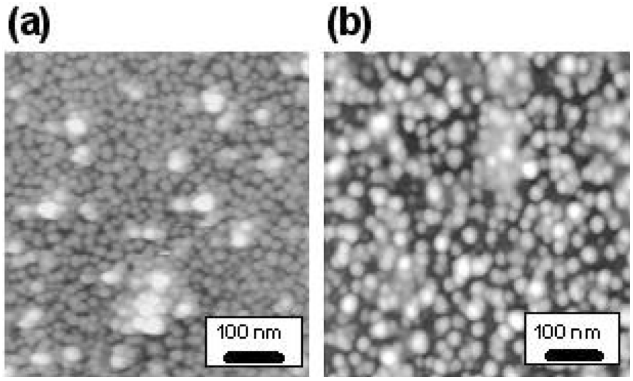

Fig. 5. 600×600 nm^2 AFM images of nanodots grown on the SiO_2/Si substrates by using NO_2 as the oxygen source. (a) ZnO nanodots grown at 450°C for 90 s and (b) ZnO nanodots grown at 550°C for 90 s.

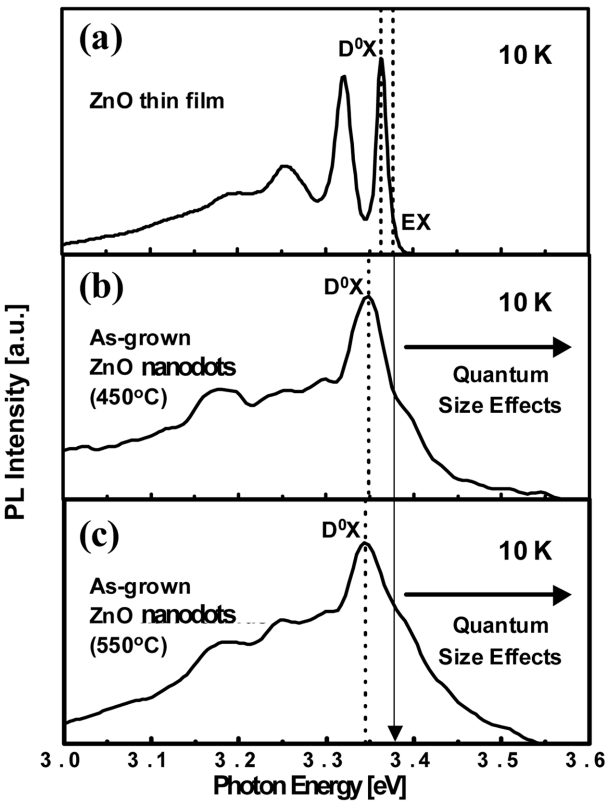

Fig. 6. PL spectra, measured at 10 K, of the ZnO thin film and nanodots grown on the SiO_2/Si substrates by using NO_2 as the oxygen source. (a) ZnO thin film grown at 550°C for 60 min, (b) ZnO nanodots grown at 450°C for 90 s, and (c) ZnO nanodots grown at 550°C for 90 s.

(grown at 550°C for 60 min) and two ZnO dot samples (grown at 450 and 550°C for 90 s) on the same SiO_2/Si substrates represented at Fig. 5, respectively, are presented in Fig. 6. In the PL spectrum from the ZnO thin film, a shoulder peak at 3.377 eV labeled "EX" and a sharp peak labeled "D^0X" are attributed to the free exciton emission and the neutral donor-bound exciton emission, respectively. For the ZnO nanodots, the broad emission band was observed with a tail up to about 3.55 eV located at the higher energy with respect to band edge emission of ZnO thin films where the EX is generally located at about 3.377 eV. This is an indication that the experimentally observed band-gap enhancement results from low-dimensional quantum confinement effects in ZnO nanodots grown by MOCVD on SiO_2/Si substrates. In addition, RT stimulated emission from self-organized ZnO nanodots on SiO_2/Si substrates is observed.

The self-organized ZnO nanodot sample for observation of stimulated emission was grown on a SiO_2/Si (111) substrate by MOCVD with the growth condition of the ZnO nanodots. The ZnO nanodots with 32-nm maximum diameter, 12-nm maximum height, both were measured by AFM, and over 9×10^{10} cm^{-2} density were grown by the condition. The ZnO thin film with a thickness of 100 nm was also prepared for this work in order to allow comparative and systematical studies on these samples. Under continuous wave He-Cd excitation at RT the EX band from both the thin film and the dot sample was dominant without any deep-level emission. On the other hand, when the optical pumping was introduced using the frequency-tripled output (355 nm, 10 ns) from a pulsed mode-locked Nd : YAG laser operating at a repetition rate of 10 Hz, broad spontaneous emission below a threshold was observed in both the thin film and the dot sample. With increase of the excitation density from 4.1 to 63.5 mJ/cm^2, the broad emission band around 3.21 eV by Nd : YAG laser excitation was clearly observed, which originates from the free exciton. Below excitation density of 40 mJ/cm^2, the integrated emission intensity showed the linear dependence on excitation intensity, which indicates spontaneous emission processes. At excitation densities of 40 mJ/cm^2, a rapid line-width narrowing of the emission band was observed. However, in spite of the narrowing of the emission, the integrated emission intensity shows the quasi-linear dependence on excitation density, namely, amplified spontaneous emis-

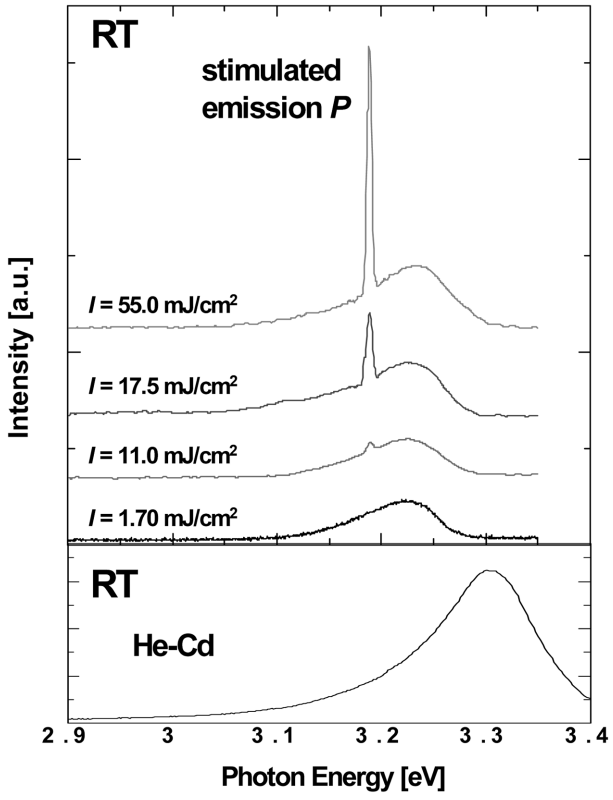

Fig. 7. RT emission spectra of the ZnO nanodots on SiO_2/Si pumped using the frequency-tripled output of the mode-locked Nd : YAG laser at various pumping intensities.

sion-like behavior.

Under continuous wave He-Cd excitation the emission band position of EX from ZnO nanodots is around 3.31 eV at RT, which is somewhat located at higher energy position than that of the expected energy of the free exciton from ZnO thin films. When the optical pumping was introduced using the Nd:YAG laser, broad spontaneous emission peaking at about 3.22 eV below excitation density of 11 mJ/cm^2 was observed as shown in Fig. 7. With increasing the optical pumping intensity to excite carriers above a threshold value, *e.g.*, 12 mJ/cm^2 per pulse, a sharp single *P* band emerged at 3.18 eV directly from the broad spontaneous emission band. With further increase of the excitation density, the intensity of the *P*-band emission was superlinearly increased with increasing the pumping intensity, while the broad spontaneous EX band located at higher energy position compared to that of the *P*-emission band showed the sublinear dependence of the PL intensity. The peak position of *P* band is constant with the pumping intensity, while that of the EX band is blue-shifted with increasing the excitation intensity due to the band filling effect. As mentioned above, superlinear increase of the intensity of the *P* band with the increment of excitation density and no shift in its peak position show typical stimulated emission behavior. The stimulated emission *P* band is attributed to an exciton-exciton collision recombination process in which one of the excitons is scattered into $n = \infty$ because the peak position of the *P* band is independent of the optical excitation density, which can be another evidence of an excitonic origin.

Zu *et al*. [12] found that a *P* stimulated emission band can only be observed for films with an average microcrystallite size smaller than about 55 nm. In their study, they reported that the small grain size films exhibit strong luminescence of EX, while the films with microcrystallite sizes larger than 55 nm, the EX becomes much weak. From the experimental results, they suggested that the existence of an exciton-exciton collision induced *P* stimulated emission band at RT is due to a spatial confinement effect because excitons are weakly confined in the microcrystallites with an average size much larger than the excitonic Bohr radius but smaller than the excitonic coherence length result. They also suggested that the weak confinement of excitons results in a large enhancement in the exciton oscillator strength and the enhancement of oscillator strength is responsible for the stimulated emission by strong excitonic action at RT. From the point of view, the origin of the stimulated emission from the self-organized ZnO nanodots in this study might be explained by enhanced spatial excitonic confinement effects in low-dimensional structures.

5. Artificial Control of ZnO Nanodots on Patterned Substrates

In order to fabricate spatially regular arrays of nanostructures, appropriately shaped patterns were introduced into the substrate followed by MOCVD growth of ZnO into the patterns. In this work, SiO_2 (50 nm)/Si substrates were patterned in the FIB chamber to create two-dimensional (2D) arrays of nanoholes. A Ga^+ liquid-metal ion source is housed, where the beam energy was fixed at 30 keV with an ion dose of 1×10^{16} cm^{-2}. The beam currents were varied from 1 pA to 1.3 nA to control the dimensions of nanoholes engraved by FIB. Numerous sputtering conditions were examined to realize the desired nanohole profiles. Figure 8(a) and (b) show AFM images of 2D nanohole arrays patterned under a programming command of a 6 nm constant depth with varying the beam size of 100 nm and 23 nm, respectively. The large beam size leads to a short process time at the expense of diameter increase of the individual holes. Using the optimized FIB-sputtering condition we have succeeded in the formation of 2D nanohole arrays with various periodicities [750 nm (beam size: 100 nm), 190 nm (beam size: 23 nm), and 100 nm (beam size: 13 nm)] over a wide area.

Figure 8(c) and (d) show AFM images of highly aligned 2D ZnO nanodot arrays formed in FIB-engraved nanoholes with different periodicities at the MOCVD-

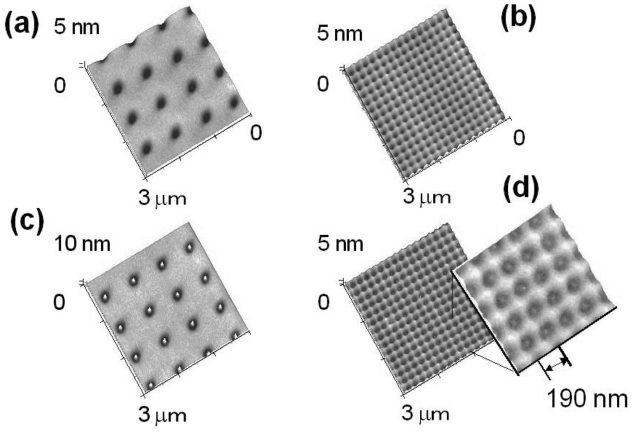

Fig. 8. Plan-view AFM images. Nanoholes have achieved under a FIB-programming command of a constant depth of 6 nm varying the beam diameter (beam current) of 100 nm [(a) 1.3 nA] and 23 nm [(b) 48 pA]. 2D ZnO nanodot arrays with different periodicities: (c) 750 nm and (d) 190 nm.

growth temperature of 700°C for 40 s, where the flow rate of DEZn was 1 μmol/min with that of N_2O being 7000 μmol/min. From the AFM study shown in Fig. 8 we could know that average heights [9 nm (c) and 5 nm (d)] and average widths [130 nm (c) and 40 nm (d)] of individual nanodots selectively grown on each nanohole array are closely related to the dimensions of the nanoholes, indicating that a nanohole with a larger dimension accommodates a larger ZnO nanodot. Perfect one-by-one accommodation of a ZnO nanodot in a nanohole was realized in the samples of 2D nanohole arrays with the 750 nm and the 190 nm periodicities, while packing percentage of ZnO nanodots in the nanoholes with the 100 nm periodicity was about 64 % in addition with large distribution in their widths.

In order to study characteristics on selective growth and evolution of ZnO nanodots as a function of MOCVD-growth time, we varied growth time from 40 s to 15 min. Figure 9 shows that that by further increase of MOCVD-growth time nanodots are converted to nanorods (15 min) on FIB-nanopatterned holes. Increase of an average dot width was a linear function on growth time, while an average dot height was less sensitive to growth time. When sufficient growth time (over 600 s) was given, the average volume of grown ZnO nanostructures increased superlinearly with increment of growth time, resulting in the formation of rod structures with random growth directions. The superlinear increase of the volume is due to preferential growth directions of the ZnO nanostructures, leading to change from dots to rods with high aspect ratios as a function of growth time. This fact indicates that FIB-patterned nanoholes acted as seeds for growth of ZnO nanodots and nanorods as a function of MOCVD-growth condition.

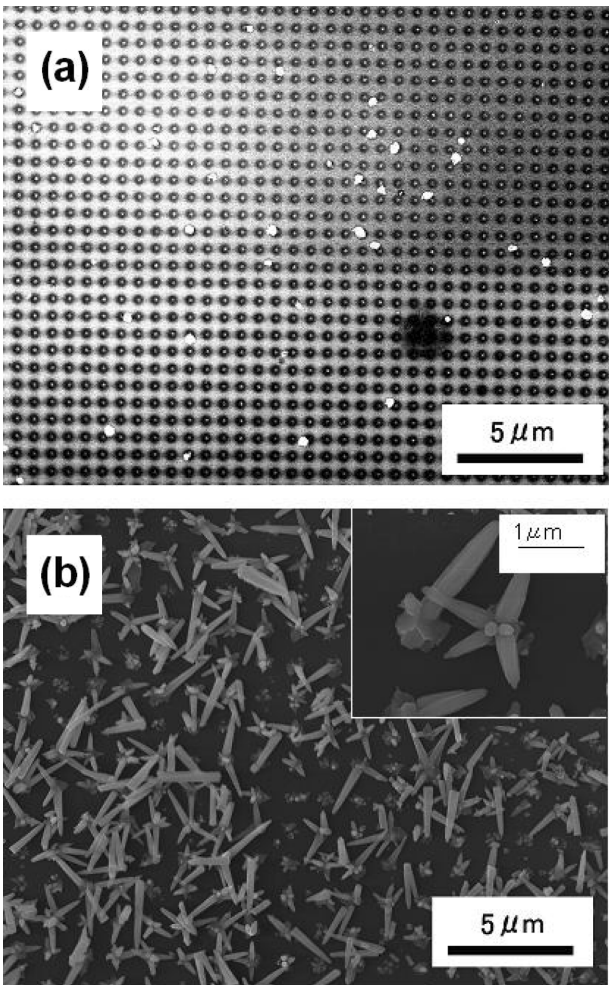

Fig. 9. FE-SEM images of selectively grown ZnO nanodots (a) and nanorods (b). The inset in (b) is a magnified image of (b).

The reliable formation of artificially controlled ZnO nanodot arrays is due to formation mechanisms responsible for initial nucleation. Considering amorphous nature of SiO_2, the selective formation of ZnO nanodots in FIB-nanopatterned SiO_2 areas is not discussed in terms of the change of the surface structure such as the generation of surface atomic steps and kinks. Instead it may be suggested that one of the plausible keys is the accumulation and diffusion of Ga atoms produced by FIB. Recently, Kammler *et al.* [24] showed that the selective formation of Ge islands on FIB-micropatterned Si (001) surfaces could be realized without modifying surface morphologies in the patterning condition with a dose as low as 6000 Ga^+ ions per 100-nm spot. They suggested that the selective formation of Ge islands is due to chemical effects of the implanted ions or strain fields of buried defects. In addition, they found that Ga^+ ion irradiation and thermal annealing allowed direct control of individual Ge island nucleation sites by a surfactant effect of the implanted Ga. Based on their suggestions, it is expected in our experiments that Ga atoms diffuse along the nanopatterns during the MOCVD growth and form the preferential nucleation sites, followed by the formation of ZnO nanodot arrays in the FIB-nanopatterned places. Based on this suggestion, it is expected in the present experiments that Ga atoms introduced during the FIB-nanoengraving diffuse along the nanopatterned SiO_2 surface during the substrate pretreatment before the main MOCVD growth of ZnO and form the preferred nucleation centers, followed by the formation of selectively grown ZnO nanodots in the patterned areas.

In an energy dispersive x-ray (EDX) result measured by an EDX spectrometer attached to FE-SEM the peaks associated with Zn, Ga, Si, and O were observed from the selectively grown 2D ZnO nanodot arrays on FIB-

patterned SiO_2. The Ga-related peaks, though it appeared at a shoulder of the Zn-related peak, suggest that Ga atoms are incorporated into the patterned area during the FIB-nanoengraving. From this result, it could be concluded that the reliable formation of self-organized ZnO nanodot arrays on functionalized substrates is mainly due to incorporated Ga ions which act as artificial traps for Zn adatoms. It can be expected in this study that the incorporated Ga atoms become preferred nucleation centers themselves, followed by the formation of highly ordered ZnO nanodot arrays in the FIB-patterned areas.

6. Conclusions

Fabrication and characterization of ZnO thin films on Si and SiO_2 substrates by MOCVD as fundamental study to realize ZnO nanostructures was carried out. The ZnO grown directly on Si without any buffer layer at the temperatures of over 500°C by MOCVD shows dominant band edge emission together with very weak deep emissions even at RT in PL measurements and high-quality crystallinity, which indicates that MOCVD is an efficient technique for fabrication of ZnO thin films. In addition, self-organized ZnO nanodots with low-dimensional quantum characteristics were synthesized by MOCVD on SiO_2/Si substrates using three-dimensional growth behavior of ZnO on SiO_2. Dot density of 10^9~10^{11} cm^{-2} can be easily controlled by varying the growth conditions. Nonlinear optical properties of the self-organized ZnO nanodots at RT were also investigated. Finally, artificial control of ZnO nanodots on substrates nanopatterned by a FIB technique was carried out. Well-ordered ZnO nanodot arrays with uniform size distributions were successfully realized by the combination of "top-down (FIB)" and "bottom-up (MOCVD)" approaches.

References

[1] K. Hummer, "Interband Magnetoreflection of ZnO", Phys. Status Solidi B 56 (1973) 249.

[2] K. Sakurai, T. Kubo, D. Kajita, T. Tanabe, H. Takasu, Sz. Fujita and Sg. Fujita, "Blue photoluminescence from ZnCdO films grown by molecular beam epitaxy", Jpn. J. Appl. Phys. 39 (2000) L1146.

[3] T. Makino, Y. Segawa, M. Kawasaki, A. Ohtomo, R. Shiroki, K. Tamura, T. Yasuda and H. Koinuma, "Band gap engineering based on $Mg_xZn_{1-x}O$ and $Cd_yZn_{1-y}O$ ternary alloy films", Appl. Phys. Lett. 78 (2001) 1237.

[4] A. Ohtomo, M. Kawasaki, T. Koida, K. Masubuchi, H. Koinuma, Y. Sakurai, Y. Yoshida, T. Yasuda and Y. Segawa, "$Mg_xZn_{1-x}O$ as a II-VI widegap semiconductor alloy", Appl. Phys. Lett. 72 (1998) 2466.

[5] D.C. Reynolds, D.C. Look and B. Jogai, "Optically pumped ultraviolet lasing from ZnO", Solid State Commun. 99 (1996) 873.

[6] T. Shiosaki, T. Shiosaki, M. Adachi and A. Kawabata, "Sputtering and chemical vapour deposition of piezoelectric ZnO, AlN and $K_3Li_2Nb_5O_{15}$ films for optical waveguides and surface acoustic wave devices", Thin Solid Films 96 (1982) 129.

[7] K. Ellmer, F. Kudella, R. Mientus, R. Schieck and S. Fiechter, "Influence of discharge parameters on the layer properties of reactive magnetron sputtered ZnO : Al films", Thin Solid Films 247 (1994) 15.

[8] M. Izaki and T Omi, "Transparent zinc oxide films chemically prepared from aqueous solution", J. Electrochem. Soc. 144 (1997) L3.

[9] K. Ueda, H. Tabata and T. Kawai, "Magnetic and electric properties of transition-metal-doped ZnO films", Appl. Phys. Lett. 79 (2001) 988.

[10] J.M. Hvam, G. Blattner, M. Reuscher and C. Klingshirn, "The biexciton levels and nonlinear optical transitions in ZnO", Phys. Status Solidi B 118 (1983) 179.

[11] D.M. Bagnall, Y.F. Chen, Z. Zhu, T. Yao, M.Y. Shen and T. Goto, "High temperature excitonic stimulated emission from ZnO epitaxial layers", Appl. Phys. Lett. 73 (1998) 1038.

[12] P. Zu, Z.K. Tang, G.K.L. Wong, M. Kawasaki, A. Ohtomo, H. Koinuma and Y. Segawa, "Ultraviolet spontaneous and stimulated emissions from ZnO microcrystallite thin films at room temperature", Solid State Commun. 103 (1997) 459.

[13] A. Ohtomo, K. Tamura, M. Kawasaki, T. Makino, Y. Segawa, Z.K. Tang, G.K.L. Wong, Y. Matsumoto and H. Koinuma, "Room-temperature stimulated-emission of exciton in ZnO/(Mg, Zn)O superlattices", Appl. Phys. Lett. 77 (2000) 2204.

[14] H.D. Sun, T. Makino, Y. Segawa, M. Kawasaki, A. Ohtomo, K. Tamura and H. Koinuma, "Biexciton emission from $ZnO/Zn_{0.74}Mg_{0.26}O$ multiquantum wells", Appl. Phys. Lett. 78 (2001) 3385.

[15] C.H. Chia, T. Makino, K. Tamura, Y. Segawa, M. Kawasaki, A. Ohtomo and H. Koinuma, "Confinement-enhanced biexcition binding energy in ZnO/ZnMgO multi-quantum wells", Appl. Phys. Lett. 82 (2003) 1848.

[16] Z.W. Pan, Z.R. Dai and Z.L. Wang, "Nanobelts of semiconducting oxides", Science 291 (2001) 1947.

[17] M.H. Huang, S. Mao, H. Feick, H. Yan, Y. Wu, H. Kind, E. Weber, R. Russo and P. Yang, "Room-temperature ultraviolet nanowire nanolasers", Science 292 (2001) 1897.

[18] Y. Li, G.W. Meng, L.D. Zhang and F. Phillipp, "Ordered semiconductor ZnO nanowire arrays and their photoluminescence properties", Appl. Phys. Lett. 76 (2000) 2011.

[19] D. Leonard, M. Krishnamurthy, C.M. Reaves, S.P. Denbaars and P.M. Petroff, "Direct formation of quantum sized dots from uniform coherent islands of InGaAs in GaAs", Appl. Phys. Lett. 63 (1993) 3203.

[20] H.-C. Ko, D.-C. Park, Y. Kawakami, Sz. Fujita and Sg. Fujita, "Self-organized cdse quantum dots onto cleaved

GaAs (110) originating from stranski-krastanow growth mode", Appl. Phys. Lett. 70 (1997) 3278.
[21] D.R. Lide, "CRC handbook of chemistry and physics", 80th ed., D. R. Lide, Ed. (CRC Press, Inc., Fla, 1999) p.8.
[22] K. Ogata, S.-W. Kim, Sz. Fujita and Sg. Fujita, "ZnO growth on Si substrates by metalorganic vapor phase epitaxy", J. Cryst. Growth 240 (2002) 112.
[23] K. Iwata, P. Fons, S. Niki, A. Yamada, K. Matsubara, K. Nakahara, T. Tanabe and H. Takasu, "ZnO growth on Si by radical source molecular beam epitaxy", J. Cryst. Growth 214/215 (2000) 50.
[24] M. Kammler, R. Hull, M. C. Reuter and F. M. Ross, "Lateral control of self-assembled island nucleation by focused-ion-beam micropatterning", Appl. Phys. Lett. 82 (2003) 1093.